

Joint use of remote sensing data and volunteered geographic information for exposure estimation: evidence from Valparaíso, Chile

Christian Geiß¹ · Anne Schauß^{1,4} · Torsten Riedlinger¹ ·
Stefan Dech¹ · Cecilia Zelaya² · Nicolás Guzmán² ·
Mathías A. Hube³ · Jamal Jokar Arsanjani⁴ ·
Hannes Taubenböck¹

Received: 20 October 2015 / Accepted: 2 November 2016
© Springer Science+Business Media Dordrecht 2016

Abstract The impact of natural hazards on mankind has increased dramatically over the past decades. Global urbanization processes and increasing spatial concentrations of exposed elements induce natural hazard risk at a uniquely high level. To mitigate affiliated perils requires detailed knowledge about elements at risk. Considering a high spatiotemporal variability of elements at risk, detailed information is costly in terms of both time and economic resources and therefore often incomplete, aggregated, or outdated. To alleviate these restrictions, the availability of very-high-resolution satellite images promotes accurate and detailed analysis of exposure over various spatial scales with large-area coverage. In the past, valuable approaches were proposed; however, the design of information extraction procedures with a high level of automatization remains challenging. In this paper, we uniquely combine remote sensing data and volunteered geographic information from the OpenStreetMap project (OSM) (i.e., freely accessible geospatial information compiled by volunteers) for a highly automated estimation of crucial exposure components (i.e., number of buildings and population) with a high level of spatial detail. To this purpose, we first obtain labeled training segments from the OSM data in conjunction with the satellite imagery. This allows for learning a supervised algorithmic model (i.e., rotation forest) in order to extract relevant thematic classes of land use/land cover (LULC) from the satellite imagery. Extracted information is jointly deployed with information from the OSM data to estimate the number of buildings with regression techniques (i.e., a multi-

✉ Christian Geiß
christian.geiss@dlr.de

¹ German Aerospace Center (DLR), German Remote Sensing Data Center (DFD), Münchner Straße 20, 82234 Oberpfaffenhofen-Weßling, Germany

² Chilean Navy Hydrographic and Oceanographic Service (SHOA), Errázuriz Echaurren 254 Playa Ancha, Valparaíso, Chile

³ Pontificia Universidad Católica de Chile and National Research Center for Integrated Natural Disaster Management CONICYT/FONAP/15110017, Vicuña Mackenna, 4860 Santiago, Chile

⁴ Heidelberg University, GIScience Research Group, Berliner Straße 48, 69120 Heidelberg, Germany

linear model from ordinary least-square optimization and a nonlinear support vector regression model are considered). Analogously, urban LULC information is used in conjunction with OSM data to spatially disaggregate population information. Experimental results were obtained for the city of Valparaíso in Chile. Thereby, we demonstrate the relevance of the approaches by estimating number of affected buildings and population referring to a historical tsunami event.

Keywords Exposure · Risk · Vulnerability · Remote sensing · Volunteered geographic information · Land-use–land-cover classification · Object-based image analysis · Rotation forest · Population disaggregation · Tsunami

1 Introduction

Various natural hazards pose major threats on mankind in particular with respect to social and economic aspects. To mitigate affiliated perils determines the accurate quantification of natural hazard risk. Thereby, natural hazard risk can be characterized based upon three distinguishable components: hazard, exposure, and vulnerability (UNDRO 1979). In this paper, we focus on the quantification of exposure. In contrast to the fuzzy concept of vulnerability (Timmermann 1981; Cutter 2003; Thywissen 2006), exposure can be considered as a highly tangible component of risk: It comprises the assets potentially affected by a hazardous event comprising people, properties, infrastructure, or economic activities (Schneiderbauer and Ehrlich 2004; Geiß and Taubenböck 2013).

In general, it is very challenging to constantly monitor exposure for highly variable urban environments (Taubenböck et al. 2012; Wieland et al. 2012a). Moreover, only exposure information with a high level of spatial detail enables the consideration of natural hazards within an affiliated risk model on a small scale (Wieland et al. 2012b). Recently, the use of remote sensing was identified as a valuable source of information for exposure estimation (Taubenböck et al. 2008). Especially latest generation optical sensors enable the detection and characterization of objects of built environments within hazard-prone areas (Ehrlich and Tenerelli 2013). For instance, Ehrlich et al. 2010, 2013 focus on the extraction and characterization of the exposed building stock using optical remote sensing data, whereas Aubrecht et al. (2013) show the estimation of human exposure on multiple spatial scales under the consideration of various earth observation data.

Nevertheless, the development of procedures for information extraction from remote sensing imagery with a high level of automatization remains a major challenge. To extract relevant information from the imagery (e.g., building footprints), the concept of supervised classification approaches (Chen and Ho 2008; Camps-Valls et al. 2014) is based on the idea to infer a rule (e.g., a decision function) from limited but properly encoded prior knowledge (i.e., labeled samples) to assign a class label to unlabeled instances of the domain under analysis. These methods became state-of-the-art processing techniques due to their favorable accuracy and robustness properties. However, the collection of appropriate prior knowledge (by e.g., detailed in situ surveys) is reported to be the most time-consuming and expensive aspect with respect to data processing. So far, researchers responded in several ways to alleviate the burden associated with a proper compilation of prior knowledge. On the one hand, approaches were designed that encode some knowledge from the unlabeled data also by means of a semi-supervised method to possibly gain viable accuracies with a

very limited number of labeled samples (Bruzzone et al. 2006). On the other hand, so-called active learning strategies were followed recently (Tuia et al. 2009b, 2011a, b). Such methods deploy predefined heuristics to rank unlabeled instances in the domain under analysis that can be considered the most valuable for improvement in estimation accuracy of a preliminary trained learning machine. Latest approaches also include the spatial domain for this task (Stumpf et al. 2014; Pasolli et al. 2014) and consider labeling costs emerging from ground surveys (Demir et al. 2014). In addition, methods to identify only a limited amount of desired (target) classes, disregarding all other existing classes in the domain under analysis, were postulated (Marconcini et al. 2014; Mack et al. 2014). Although labeling costs can be reduced compared to simple fully supervised methods, all considered methods determine a considerable amount of data collection.

In parallel, a new mechanism for the user-generated acquisition and compilation of geographic information, termed volunteered geographic information (VGI) (Goodchild 2007), evolved within the past years. Those kinds of data comprise mainly vector data such as digital maps with further thematic information content but also georeferenced ground-based imagery, among others. Those are made publicly available through web-based distribution mechanisms. For instance, the OpenStreetMap (OSM) project is one of the most popular examples of VGI with a growing perspective as outlined in Jokar Arsanjani et al. (2015a). The project was initiated in 2004 and hosted at University College London with the aim to create a free digital editable vector map of the world (Haklay 2010). Thereby, information is collected currently by up to 2.2 million participants, compiled within a central database, and distributed in multiple digital formats through the World Wide Web as “open data” according to the Open Data Commons Open Database License (OSM 2015a). The deployment of VGI for data analysis procedures and substitution of traditional data sources was identified as a promising application field (Sester et al. 2014). Thereby, new challenges are related to the heterogeneity of the data and assurance of data quality (Flanagan and Metzger 2008; Haklay 2010; Jokar Arsanjani et al. 2015b). Accordingly, recent research focused on the assessment of quality properties in order to evaluate suitability for different application fields (Neis and Zipf 2012; Hecht et al. 2013; Fan et al. 2014; Jokar Arsanjani et al. 2015c).

So far, VGI was rarely used in conjunction with remote sensing data to enable advanced data processing procedures. Recent attempts deploy OSM data for enhanced mapping and characterization of built environments (Klonner et al. 2014; Kunze and Hecht 2015). In addition, for example, Foody and Boyd (2013) and Pesaresi et al. (2013) deploy OSM data for validation of information derived from remote sensing imagery. In the context of natural hazard risk research, Schnebele and Cervone (2013) and Poser and Dransch (2010) aim to extract relevant information with respect to hydrological hazards.

In contrast to previous approaches that combine remote sensing and VGI, here, we uniquely deploy OSM data for supervised extraction of land-use/land-cover (LULC) information from very-high-resolution (VHR) multispectral imagery. We do so to subsequently estimate crucial exposure components (i.e., number of buildings and population) with a high spatial detail and high level of automatization. In particular, first, we compute a measure from the OSM metadata to assess the quality of the data. Quality properties of the data are subsequently considered for a spatially stratified selection of labeled training geometries. In parallel, VHR imagery is subject to image segmentation (Blaschke 2010), and OSM geometries are combined with the remote sensing data based on an object-based fusion scheme. We characterize the objects in the remote sensing imagery via a high-dimensional feature space by exploiting again techniques of object-based image analysis (OBIA). Those kinds of approaches were demonstrated to be beneficial compared to per-

pixel processing techniques for data with a considerable higher spatial resolution than the objects to be extracted from the data (Blaschke 2010). Based on the derived information, we identify LULC by using advanced machine learning techniques. In particular, a rotation forest approach (Rodriguez et al. 2006) was deployed to alleviate the computational burden frequently associated with the selection of appropriate features for classification (based on, e.g., filter or wrapper methods) and to simultaneously ensure favorable accuracy properties. The urban LULC information is jointly deployed with OSM data to estimate the number of buildings using regression techniques. Analogously, urban LULC information is used in conjunction with OSM data to spatially disaggregate population information. Experimental results are obtained for the city of Valparaíso in Chile. The city is prone to various natural hazards such as earthquakes, tsunamis, and landslides. Consequently, we show the relevance of the approach by estimating number of affected buildings and population referring to a historical tsunami scenario.

The remainder of the paper is organized as follows: We provide a brief description of the study site and incorporated data in Sect. 2. Section 3 documents the developed and deployed methods for information extraction and exposure estimation, whereas Sect. 4 contains affiliated results and discussion. Conclusions and future perspectives are outlined in Sect. 5.

2 Study site and data

2.1 Valparaíso

Valparaíso ($33^{\circ}2' S$, $71^{\circ}37' W$) is located on the Pacific Coast in the Western part of Chile (Fig. 1a). It is one of the largest coastal cities of Chile and features approximately $>280,000$ inhabitants (INE 2015). The city is prone to a number of hazards, whereby it is heavily threatened by earthquakes and tsunamis. The Nazca plate plunges beneath the continental South American plate. The geographic location of Valparaíso right beside the sea and geological characteristics (i.e., seismic amplification due to soft soil) makes the city especially prone to them (Fig. 1b). A very destructive earthquake took place in 1906 and hit Valparaíso with a magnitude M_w of 8.3. Since then, there were 12 earthquakes affecting Valparaíso with an intensity larger than seven (Indirli et al. 2010). Majority of them had their epicenter offshore of Valparaíso along the plate boundary. Three of them were also tsunamigenic (i.e., the events in 1906, 1918, and 1985). In addition, there is a considerable landslide risk, especially in case of heavy rainfalls due to soil materials, steep slopes within the settlement area, and deep fluvial incisions. Risk of fires is also exigent and worsened by windy weather, hill roads, which are hard to access, dominance of wooden houses, and sometimes insufficient water pressure in the hydrants. Recent examples are the forest fires that occurred in April 2014, which could not be stopped for several days (April 12th–17th). Almost 1000 hectares were burnt. The fires devastated about 3000 houses in 12 districts and affected 13,000 people (ONEMI 2014). In general, the urban morphology of Valparaíso determines two sectors with distinct risk properties (Fig. 1c–d). The harbor area, characterized by port facilities and commercial districts, is highly exposed to tsunami hazards and destructive effects of earthquakes, whereas the hill quarters, covered by small and squat houses, are in particular subject to risks related to landslides and fires.

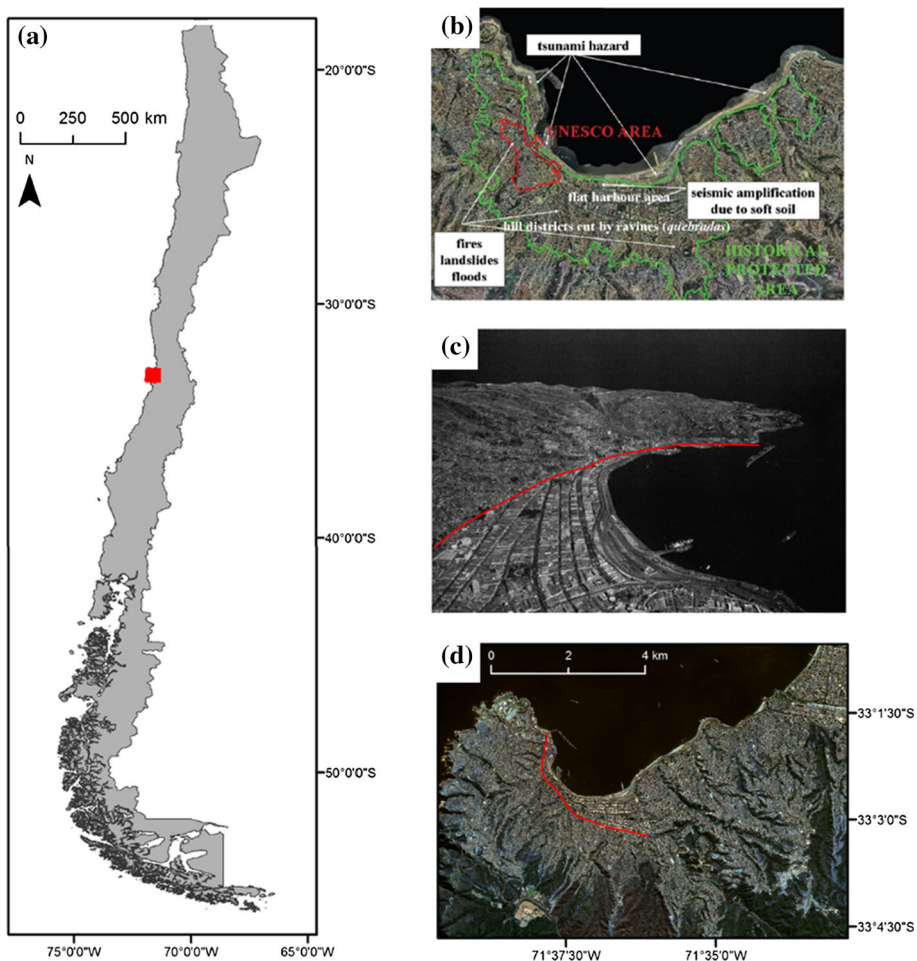


Fig. 1 Overview on the location of the study area and acquired remote sensing data. **a** The location of Valparaíso in Chile; **b** Indication of hazards and safeguarded areas (green area: historical protected area; red area: UNESCO protected historical center); **c** Distinct urban morphology of Valparaíso (imagery taken from Sánchez et al. 2009)—red line indicates the distinction of flat harbor area along the coast and hill quarters; **d** Worldview-2 imagery [red line simultaneously used as in (c)]

2.2 Data

2.2.1 Multispectral imagery from WorldView-2

In this study, multispectral imagery from the WorldView-2 sensor is deployed (Fig. 1d). Since 2009, the system operates on a sun-synchronous orbit at an altitude of 770 km with an average revisit capability of 1.1 days. The sensor provides imagery with a ground sampling distance of up to 0.46 m for the panchromatic band and 1.85 m for the multispectral bands (DigitalGlobe 2010). Here, we used imagery with four bands (i.e., blue 0.450–0.510 µm; green 0.510–0.580 µm; red 0.630–0.690 µm; nir 0.770–0.895 µm), which was acquired on April 19, 2014.

2.2.2 OpenStreetMap

For the subsequent compilation of training segments, we acquired OSM data for Chile from the provider Geofabrik (2014) on November 4, 2014. Data are compiled according to eight feature categories, i.e., “Points of Interest” (POIs), places, roads, railways, waterways, natural, land use, and buildings (OSM 2015b). To assess the quality of the acquired data, we subsequently use metadata from the OSM planet file (OSM 2015c). Such information reveals attributes about the history of the individual objects such as a User ID, time of last edit, or the number of edits per object (Jokar Arsanjani et al. 2015a, b, c). Notably, those information reveal that most object within our study site were added in April 2014. This is congruent with the time interval of the occurrence of the devastating fires mentioned before. The vast majority of building footprint geometries of Valparaíso was generated within the activity of two Humanitarian OpenStreetMap Team tasks, which aimed to map the areas affected by the disaster as they were before the fires in order to support damage assessment and humanitarian response activities (OSM Task Manager 2014a, b) in a timely manner. In turn, this also documents how specific events trigger the continuation of global VGI but also show that large parts of the world feature incomplete VGI with respect to spatial coverage (see also Sect. 3.1).

2.2.3 Census data

To spatially disaggregate population numbers, we deploy census data from the National Statistics Institute of Chile (INE). A census was conducted approximately every ten years since the first census in 1813. The last census was carried out in 2012; however, data were retracted due to inaccuracies during acquisition and processing (Bianchini et al. 2013). Accordingly, we use data from the 2002 survey, which provides de facto information about population at their place of residence. Data are aggregated according to four spatial levels [i.e., “comuna” (municipality), “distritos censales” (census districts), “zonas censales” (census zones), and “manzanas” (building blocks)], reaching from a coarse aggregation level (“comuna”) to a very fine one (“manzanas”).

3 Methods

To estimate exposure, we carried out a sequential procedure with four main steps (Fig. 2) dedicated to (i) proper preprocessing of the data (Sect. 3.1); (ii) a highly automated supervised classification approach for extraction of (urban) LULC (Sect. 3.2); and estimation of exposure (Sect. 3.3) comprising (iii) the number of buildings and (iv) population.

3.1 Preprocessing

WorldView-2 imagery was subject to orthorectification and atmospheric correction using the methodology of ATCOR-2 (atmospheric and topographic correction for satellite imagery; Richter 1996; Richter and Schläpfer 2014). For the LULC classification, five different thematic classes of geometries were compiled from the OSM data. In particular, geometries for the classes “buildings”, “roads”, “trees/bushes”, “meadow”, “water” were generated based on the OSM categories “buildings”, “roads”, “land use”, and “natural”. To correspond to the taxonomy of classes frequently deployed in (urban) LULC

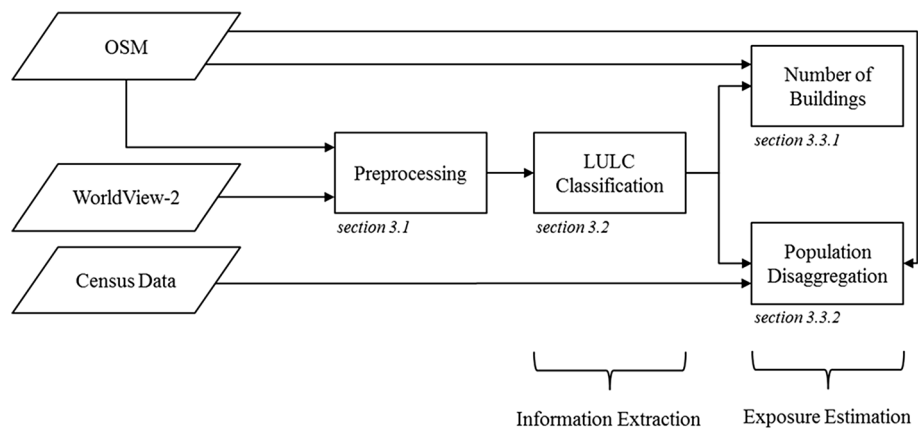


Fig. 2 Overview of processing steps

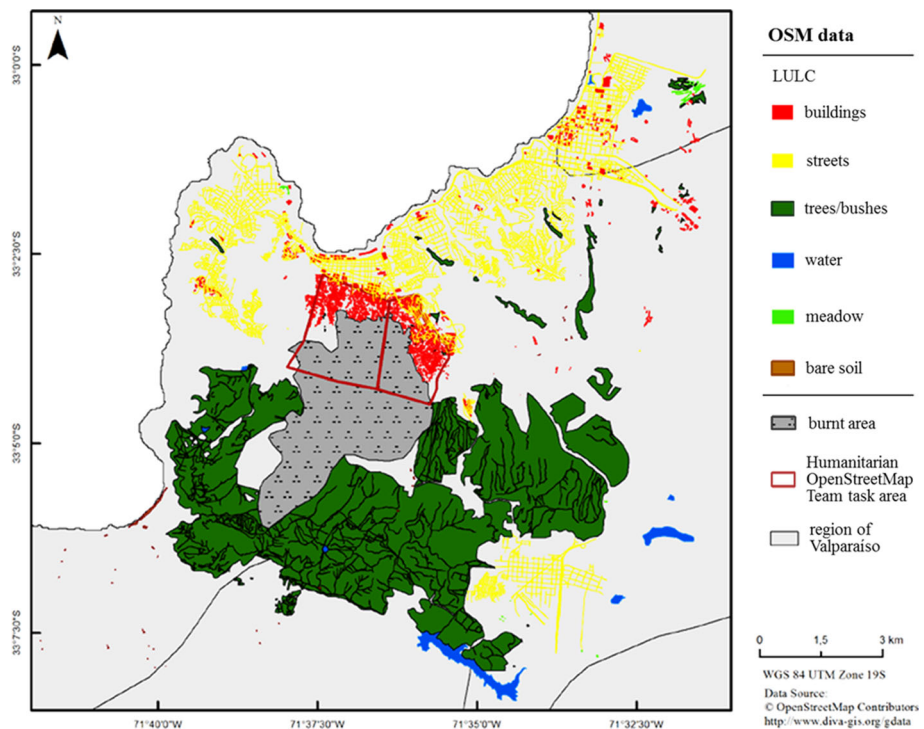


Fig. 3 Overview of available OSM data according to different LULC classes; areas of the two Humanitarian OpenStreetMap Team tasks and the area, which was burnt by the fires during April 2014 (Sect. 2.2.2), are also indicated

classification, we added geometries for the class “bare soil”, since there was no related information available in the OSM data for our study site. We ensured positional accuracy of the vector data, carried out consistency checks, and excluded unsuitable information by

means of automated procedures. The final available vector data from OSM are visualized in Fig. 3.

3.2 Information extraction

A first crucial step in estimating exposure information from VHR satellite imagery is the extraction of a detailed built-up mask that provides information about the location of buildings and the area occupied by buildings. Therefore, a detailed LULC map was derived. For this purpose, a hierarchical supervised classification approach was designed (Fig. 4). First, WorldView-2 imagery was subject to multi-scale segmentation and exhaustive feature calculation (Sect. 3.2.1). Then, segments of WorldView-2 imagery were fused with OSM geometries to obtain labeled segments for training a supervised classification model. In addition, measures were computed from the OSM data in order to evaluate the quality of the data for a spatially stratified selection of most viable training segments. Thereby, plausibility rules were introduced to ensure a reliable selection of training segments (Sect. 3.2.2). The actual supervised classification task was followed by a postclassification processing procedure to further enhance classification outcomes (Sect. 3.2.3).

3.2.1 Image segmentation and feature calculation

The multispectral imagery was subject to a multi-level segmentation procedure. The use of multiple segmentation levels is motivated by the circumstance that heterogeneous objects in urban environments feature frequently several magnitudes of spatial extent. This implies that a single segmentation is not sufficient to represent all objects in the data adequately (Bruzzone and Carlin 2006). We used a bottom-up region-growing segmentation algorithm for partition of the imagery (i.e., fractal net evolution approach as implemented in the software environment eCognition; Baatz and Schäpe 2000). Thereby, an unambiguous hierarchy of segmentation levels is ensured in a way that an object at a finer segmentation level must be included in only one object at a coarser segmentation level. Consequently, the aim is not to deploy a single, possibly best level of representation of each object like in traditional approaches, but rather to model the multi-level spatial context of each object (Bruzzone and Carlin 2006; Taubenböck et al. 2010).

Different approaches were proposed in the literature to objectively identify a single, possibly best segmentation (Espindola et al. 2006; Dragut et al. 2010), or a set of multiple, possibly best segmentations (Martha et al. 2011). Additionally, Esch et al. (2008) design an

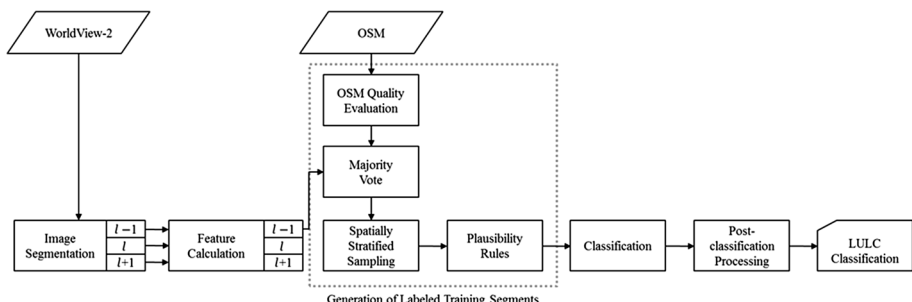


Fig. 4 Overview of proposed LULC information extraction workflow

approach to create a single multi-level segmentation layer, and Geiß et al. (2016a) jointly internalize the aforementioned concepts by proposing a procedure to create an optimized single multi-level segmentation layer objectively. However, recently it could be shown that classification accuracies are less dependent on segmentation. If undersegmentation remains at acceptable levels, imperfections in segmentation are overruled and high levels of accuracy are still achievable (Belgiu and Dragut 2014). Consequently, segmentation was carried out on three hierarchical levels (denoted as $l - 1$, l , $l + 1$; see also Fig. 4) without exhaustive optimization procedures to keep computational costs low. From a conceptual point of view, the finest level $l - 1$ comprises segments smaller than most real-world objects (oversegmentation); segments in l correspond to most real-world objects of interest; $l + 1$ comprises segments larger than most real-world objects in the image (undersegmentation) (Geiß and Taubenböck 2015). Under consideration of preliminary runs, segmentation of the multispectral bands was carried out with scale factors of 50 for $l - 1$, 150 with respect to l , and 500 regarding $l + 1$. It can be noted that segmentation results are depended on characteristics of the image data and will vary as a function of spatial resolution, number of bands, image quantization, and scene properties (Stumpf and Kerle 2011). However, an increasing scale factor will lead to larger object sizes. In addition, some further free parameters of the segmentation algorithm need to be defined. In this manner, we suggest to put more emphasize on shape heterogeneity rather than on gray-value heterogeneity. This is due to the fact that man-made features such as buildings and other objects of urban environments have distinct shape and size properties, unlike natural features. Analogously, the weights for heterogeneity of smoothness and compactness can be maintained equal (i.e., shape 0.7, color 0.5).

For characterization of the generated segments from the VHR imagery, we carried out multi-level feature calculation. Features belonging to the group of mathematical morphology (Soille 2004) were computed from the panchromatic band (*PAN_MM*), since it was shown that such derivates can encode valuable information for urban LULC classification (e.g., Soille and Pesaresi 2002; Tuia et al. 2009a; Geiß et al. 2016b). In particular, erosion, dilation, opening, closing, opening by top hat, and closing by top hat operations were carried out with linear ascending sizes of a square-shaped structuring element (SE) $B = \{5, 10, \dots, 30\}$ on the image pixels. The optical imagery was further deployed to compute measures of central tendency (*OPT_MCT*), i.e., mean and median were computed for the blue, green, red, and nir bands in addition to a brightness and maximum difference band (Stumpf and Kerle 2011). Analogously, measures of spread (*OPT_MS*), i.e., standard deviation, variance, minimum, maximum, range, and interquartile range were calculated for the four spectral bands. Two band ratios (*OPT_BR*) were further deployed to characterize vegetation activity (i.e., normalized differenced vegetation index) and enhance spectral dissimilarities between bands (i.e., red/nir) (e.g., Bruzzone and Carlin 2006; Puissant et al. 2014; Leichtle et al. 2017). To take advantage of differing shapes of individual urban LULC objects, we calculated features related to the geometry of objects. In particular, the extent of objects (*GEOM_EXT*) was characterized considering area, length, ratio of length and width, perimeter, as well as ratio of area and perimeter. In addition, the shape of objects (*GEOM_SHA*) was approximated with measures that deploy a comparison with two-dimensional geometrical forms such as square, rectangle, or ellipse (i.e., rectangular and elliptic fit, asymmetry, compactness, density, roundness, shape, and border index) as implemented in the software environment eCognition (Trimble 2014; Sun et al. 2015). Lastly, relational features (*REL*) were computed (Bruzzone and Carlin 2006). For instance, the number of objects from a finer segmentation level in relation to an object from a coarser level aims to further reflect the spatial alignment and composition of image

objects. Thereby, we exploit the relation that objects from a coarser level containing a high number of objects from a finer segmentation level indicate LULC classes with a high level of individual real-world object complexity (e.g., buildings that are composed by a variety of architectural components). Overall, each image object of level $l-1$ O_i^{l-1} is represented by a 270-dimensional feature vector

$$f(O_i^{l-1}) = \left\{ \text{PAN_MM}(O_i^{l-1})^{108}, \text{OPT_MCT}(O_i^{l-1})^{36}, \text{OPT_MS}(O_i^{l-1})^{72}, \text{OPT_BR}(O_i^{l-1})^6, \text{GEOM_EXT}(O_i^{l-1})^{15}, \text{GEOM_SHA}(O_i^{l-1})^{24}, \text{REL}(O_i^{l-1})^9 \right\} \quad i = 1, 2, \dots, N^{l-1} \quad (1)$$

where N^{l-1} denotes the number of objects at the finest segmentation level, and the superscript denotes the dimensionality of each feature group from the three segmentation levels.

3.2.2 Generation of labeled training segments

In parallel to image segmentation and feature calculation, OSM data were subject to quality evaluation to allow for a guided selection of most suitable training segments. Recently, Jokar Arsanjani et al. (2015c) proposed a so-called contribution index (CI) to assess the quality of the OSM data by analyzing spatiotemporal patterns with respect to the history and evolution of the data. It consists of four measures, which were here computed from square-shaped grid cells with an edge length of 1 km (Fig. 5). The first measure is the

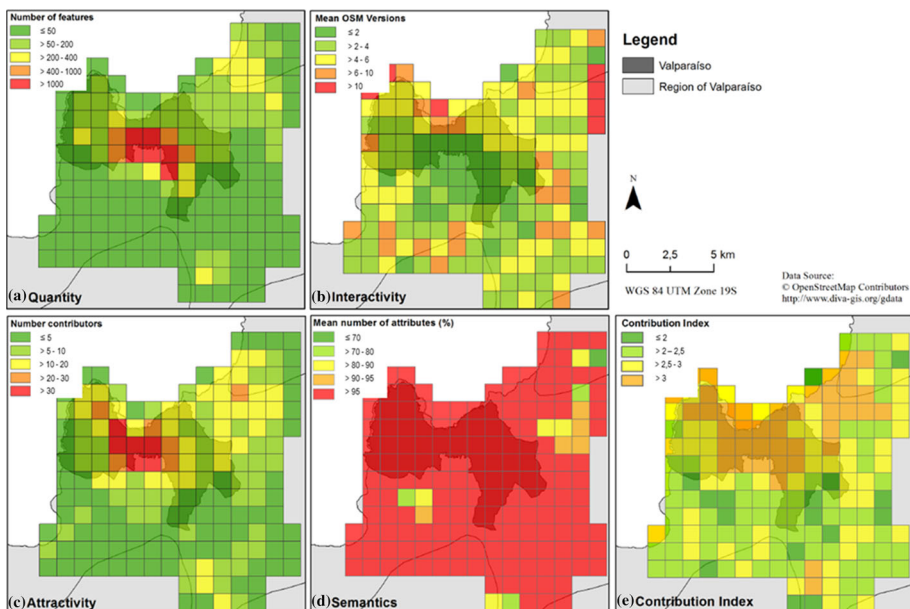


Fig. 5 Contribution index for assessing the quality of OSM data; **a** the number of nodes per cell was used to characterize the *quantity*; **b** the average number of edits made per cell indicates *interactivity*; **c** the number of users who edited nodes within a cell reflects *attractiveness*; **d** the mean number of nodes which possesses attributes per cell characterizes the *semantic content*; the combined *contribution index* is shown in **(e)**

number of nodes per cell. It is used to describe the quantity of the data. The average number of edits made per cell indicates interactivity, and the number of users who edited nodes within a cell is intended to reflect attractivity. Lastly, the semantic content shows how exhaustive the nodes within a grid cell are attributed. Thereby, the CI internalizes relationships expressed by, for example, Linus's law, which states in this application context that a larger number of volunteers contributing to the generation of the geographic information induce more exhaustive control mechanisms and, thus, a higher quality of the data. The required information was extracted from the so-called OSM "planet file". Here, the CI was computed by an averaged ordinal ranking of the individual measures. Thereby, a high numerical value indicates high quality of the OSM data, whereas low values reflect low data quality.

The CI of the region of Valparaíso shows that OSM data feature a higher quality in urban areas compared to non-urban areas. This is in accordance with finding from previous studies in other regions of the world (Zielstra and Zipf 2010; Jokar Arsanjani et al. 2015c).

In parallel, available OSM geometries were fused with segments from level $l - 1$. A segment was identified as a labeled training segment for a specific class if the segment's area was covered by >50% of the respective thematic class in the OSM geometries, what corresponds to a majority vote per segment (Fig. 6). Finally, we selected training segments as follows for the actual classification task. Cells with a high CI value (Fig. 5e) were prioritized for the selection of training segments within a spatially stratified sampling process. However, also geometries from residual cells were incorporated to avoid problems associated with a possible shift of covariance for the whole scene (Tuia et al. 2011a, b). To avoid model bias induced by class imbalance, we selected the same number of labeled

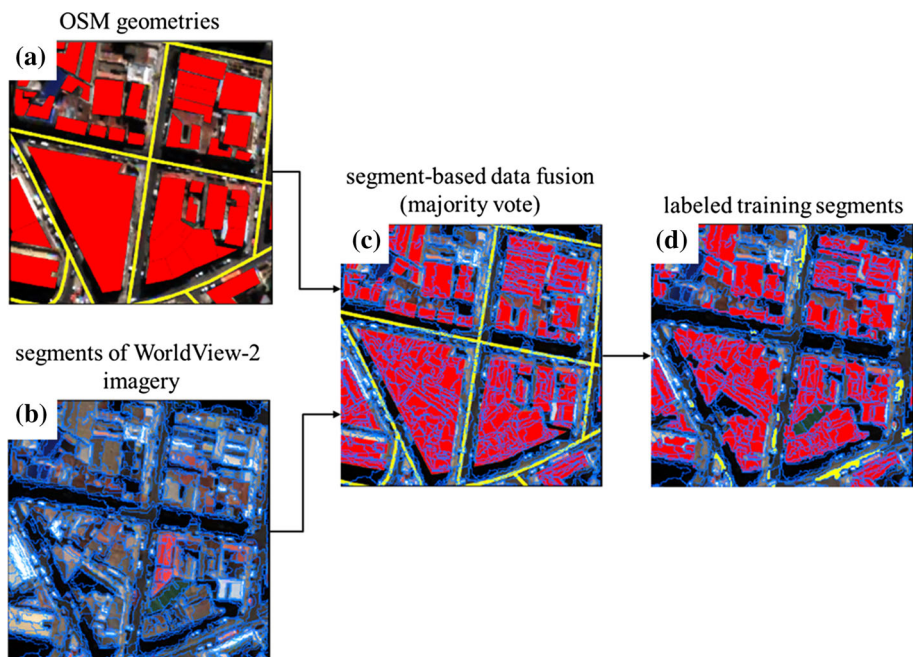


Fig. 6 Fusion scheme; **a** OSM geometries; **b** segments of satellite imagery; **c** segment-based fusion of data by majority vote; **d** labeled training segments for classification

segments per class (i.e., 600). Thereby, it can also be noted that a selection which considers the a priori probability of classes in the OSM data may generally be unlikely representative, since volunteers frequently focus on certain classes within specific application-focused compilations of OSM data (e.g., here vast majority of OSM geometries were compiled during the aforementioned Humanitarian OpenStreetMap Team tasks which focused on the class “buildings”).

Besides, the sun azimuth angle of the applied imagery of Valparaíso induced shadow areas. Naturally, such areas are not included as thematic class in the OSM data and feature a non-ubiquitous nature. Hence, shadow areas were classified from the remote sensing data with a property-based method (Adeline et al. 2013), i.e., by means of an empirically determined brightness threshold. In addition, some further plausibility rules were introduced to ensure validity of training segments. For instance, training segments corresponding to vegetation must exceed a domain-specific NDVI-related threshold. In contrast, training segments comprising impervious surface materials (i.e., buildings and roads) must fall below that NDVI-related threshold simultaneously.

3.2.3 Learning of classification model and postclassification processing

A classifier ensemble method named rotation forest (Rodriguez et al. 2006) was used for solving the actual LULC classification problem. This recently presented approach for classification problems outperformed traditional ensemble methods such as Random Forest or Bagging in terms of classification accuracy (Rodriguez et al. 2006; Kavzoglu and Colkesen 2013; Xia et al. 2014). Rotation forest is a nonparametric supervised classifier ensemble, which uses decision trees as base classifiers and employs feature extraction (i.e., rotation of the feature axes) based on principal component analysis (PCA). This principle is followed since decision trees are sensitive to axis rotations, and classifiers obtained with different rotations of a data set can be highly diverse (Stiglic et al. 2011).

The rotation forest approach employs different configurations of the set of labeled training samples. First, the feature set is split into several subsets on which the initial training set is projected. Subsequently, a sparse rotation matrix is constructed based on feature extraction on the individual subsets. The latter are subject to a bootstrap algorithm to select 75% of the initial training samples. A classifier is generated from the features projected by the rotation matrix, and a final class label is obtained according to a confidence criteria computed from the labeling results of multiple iteratively learned classifiers (Rodriguez et al. 2006; Xia et al. 2015). In the experiments, we used PCA for feature extraction in conjunction with a J48 classifier from the WEKA library (Hall et al. 2009) as base classifier and determined optimal hyperparameters (i.e., size of the ensemble and number of features in a subset) empirically with a cross-validation strategy.

Postclassification processing was carried out to further enhance classification accuracy, especially for the LULC class “buildings”, which is of vital importance for the subsequent exposure estimation efforts. Errors in the classification result can often be related to small regions with arbitrary shapes as produced by image segmentation (Zheng et al. 2014). We deployed several unambiguous context-based rules to address this problem, i.e., a singular classified segment of a certain class which is completely nested inside segments of a different class is assigned to the class of the surrounding segments (e.g., a singular image object classified as “road” is reclassified to “buildings” if it is completely surrounded by image objects of the class “buildings”).

3.3 Exposure estimation

3.3.1 Number of buildings

Complex urban environments prohibit a direct inference of number of buildings based on the presented LULC classification. This is due to the fact that extracted segments of the LULC class “buildings” do not necessarily correspond to the outline of individual building footprints. In complex urban environments such as Valparaíso, buildings are often aligned to each other with a minimum of spectral dissimilarity of neighboring roof surfaces and have complex interactions (e.g., shadow). In addition, buildings frequently feature several structural elements, which can appear as individual footprints themselves in the imagery although they are part of a single construction. This situation triggered the idea to further deploy information encoded in the OSM data for the estimation of the number of buildings. In particular, we suggest inferring an empirical relation between the number of labeled building geometries from the OSM data and affiliated building segments from the information extraction procedure (Fig. 7).

First, the imagery was subject to a renewed segmentation. There, the focus was to model segments which emphasize square-shaped properties of image objects and, thus, correspond specifically to the LULC class “buildings”. To this purpose, additional image bands were computed and jointly used with the multispectral bands for segmentation according to the setup described in Sect. 3.2.1. In particular, image bands obtained from the use of morphological operators on the panchromatic band were considered (i.e., erosion, dilation, opening, and closing with a square-shaped SE of 5 pixel diameter). This is consistent with other studies, which deploy additional image bands from morphological filtering for segmentation (e.g., Pesaresi and Benediktsson 2001; Epifanio and Soille 2007; Sheng et al. 2009). In addition, images obtained by running two different edge extraction algorithms [i.e., canny edge detector (Canny 1986) and Lee-sigma edge detection filtering (Lee 1983)] are included in the segmentation (Ali and Clausi 2001). Finally, a majority vote strategy was applied to label newly generated segments as buildings using the previous LULC class “buildings”.

For the regression approaches, we deployed a set of features (i.e., independent variables) that can be attributed to the group of landscape structure metrics (Berry 2007), which were computed from square-shaped grid cells. The size of the grid cells was chosen according a priori considerations, i.e., a trade-off between the ability to capture urban structures (edge length must not be too small) and the ability to differentiate between diverse structures (edge length must not be too large) must be maintained. Here, we chose an edge length of 0.25 km, which converges to the mean size of urban blocks according to previous empirical studies for different urban areas (Taubenböck et al. 2013). Metrics for each grid cell were calculated based on all segments newly labeled as “buildings”, which

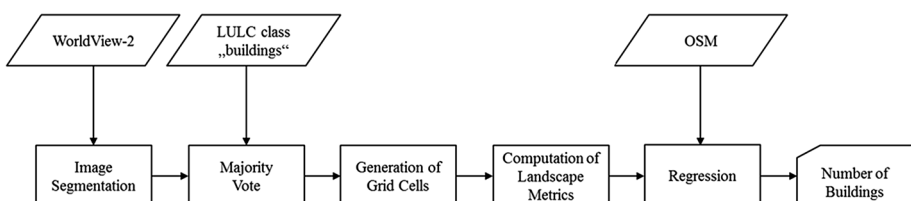


Fig. 7 Overview of proposed workflow for the estimation of number of buildings

have their centroid in the respective cell. The measures focus on the characterization of building segments with respect to their extent such as mean segment size or variation in segment size. Also relative measures such as the relative number of segments, which represents the ratio of the number of segments per grid cell and total number of segments in the study area, are considered. In addition, e.g., shape metrics are used to approximate the constructional complexity of buildings within a grid cell. Overall, 12 metrics were computed.

Regarding the actual regression task, we considered a multi-linear ordinary least squares (OLS) model and a nonlinear support vector regression (SVR) model. The OLS method minimizes the sum of squared vertical deviations between the observed values in the data set and the values predicted by the linear approximation to describe, as close as possible, the original values of the dependent variable (Montgomery et al. 2001). Instead, SVR is able to reflect nonlinear relationships (Smola and Schölkopf 2004). It is based on support vector machines (SVM), which determine a suitable set of parameters that establish a decision surface, the so-called hyperplane, between the different classes of training samples according to their position in an n -dimensional feature space. The optimal separating hyperplane is identified as the maximized margin between the different classes and the hyperplane. Detailed theoretical background of SVM can be found in Vapnik (1995), Cortes and Vapnik (1995), and Burges (1998).

In the experiments, regression models were learned from 25 grid cells, where the actual number of buildings was determined automatically from the OSM data (i.e., number of building geometries). We excluded collinear features for the OLS model and determined optimal hyperparameters with respect to minimal root-mean-squared error (RMSE) for the SVR approach (i.e., complexity parameter C and exponent of polynomial kernel) empirically with a cross-validation strategy.

3.3.2 Population disaggregation

To provide fine-scale population information, we deployed and evaluated four different disaggregation approaches based on simple areal weighting and dasymetric mapping methods. Disaggregation methods perform a transformation, which involves transforming data from one set of coarse spatial units (i.e., source zone) to one set of finer spatial units (i.e., target zone) (Wu et al. 2005). As such, we used for all approaches census data from the coarsest level (i.e., “comuna”; Sect. 2.2.3) as source zone and deployed the pixels which constitute the LULC class “buildings” as target zone, since it was assumed that people solely dwell in buildings. The disaggregation approaches are described below.

(i) Simple areal weighting (SAW)

Our baseline approach was simple areal weighting (SAW). SAW is based on the assumption that population is uniformly distributed within the source zone. Therefore, population numbers are assigned proportionally to the area of the spatial units in the target zone (linear disaggregation):

$$\text{Pop}_i = \frac{A_i}{\sum A_i} * \text{Pop} \quad (2)$$

where A_i is the area of the spatial units (i.e., pixels), $\sum A_i$ the sum of areas of all spatial units and Pop the population number of the source zone (here “comuna”).

(ii) SAW under consideration of estimated number of buildings (SAW-NB)

In addition, we used a dasymetric mapping method, which deploys knowledge of local characteristics to incorporate zones of different population densities (Mennis and Hultgren 2006). Here, dasymetric zones were generated by using ancillary information derived from the remote sensing data. In particular, the estimated numbers of buildings (Sect. 3.3.1) were used. By dividing the population of the source zone by the estimated number of buildings, the average number of inhabitants per building can be derived. By means of this information, the population can be calculated by multiplying the average number of inhabitants per buildings with the number of buildings per grid cell. In a second step, the resulting number of population per grid cell was disaggregated to pixel level by SAW. Thereby, the idea is to improve the SAW approach by constraining the population distribution beforehand based on ancillary information.

(iii) SAW and SAW-NB under consideration of OSM data

Lastly, we aimed to enhance the population disaggregation by incorporation of OSM information. For this purpose, we used land-use information other than “residential” from the OSM data to possibly identify zones, which cannot be considered equally populated although they belong to the LULC class “buildings”. OSM data contain so-called land-use objects, which represent polygons with affiliated land-use categories. In addition, so-called POIs were included, which represent punctual information indicating public, recreational, and cultural places. To use this information, the various labels were aggregated according to semantically relevant categories such as “industrial”, “gastronomy”, and “shopping”. Thereby, polygons were directly combined with segments from the LULC class “buildings”, whereby punctual information was related to corresponding segments according to a neighborhood criterion. The resulting information for Valparaíso is depicted in Fig. 8.

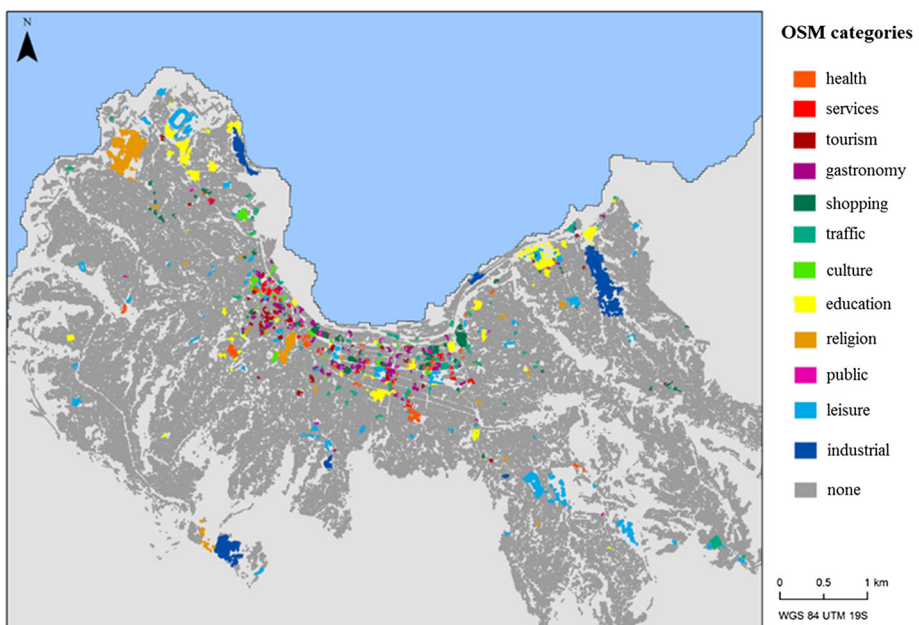


Fig. 8 OSM land-use objects and POIs aggregated according to 12 semantically relevant categories

In the experiments, we evaluated a factor of 0.5 for weighting areas of the spatial units in the target zone regarding the categories “health”, “services”, “tourism”, “gastronomy”, and “shopping”. This was done to reflect a likely mixed usage within those categories, where, for example, the ground floor of a building was used in a commercial manner and the residual floors feature residential usage. However, for the residual categories we applied a weighting factor of zero.

4 Results and discussion

4.1 Information extraction

Generalization capabilities of learned classification models are assessed with an independent test set comprising 1056 labeled segments of different LULC classes, which is compiled based on random sampling strategy and manual image interpretation. Model selection with respect to hyperparameter tuning of the rotation forest classifier is based on κ statistic (Foody 2002) as global measure for accuracy and corresponding numbers are shown in Fig. 9a. There, we test the robustness of the models with respect to available training segments per class (i.e., a varying number of samples per LULC class were drawn randomly from the set of available samples). It can be seen that κ statistics increase in a strictly monotonous way with a larger number of samples in the model. With a small number of samples, κ statistics meet a substantial agreement (i.e., mean κ statistics vary between 0.68 and 0.76). Then, a plateau is reached where only slight gains of accuracies can be realized; however, the function culminates in an excellent agreement (κ statistic >0.8) with the unreduced training set. Simultaneously, standard deviations decrease, what indicates that models become more robust.

Accuracy measures for final LULC classification after postclassification processing are depicted in Fig. 9b with affiliated LULC classification map (Fig. 9c). Both overall accuracy and κ statistic could be increased to 86.7% (+0.8%) and 0.8188 (+0.0107),

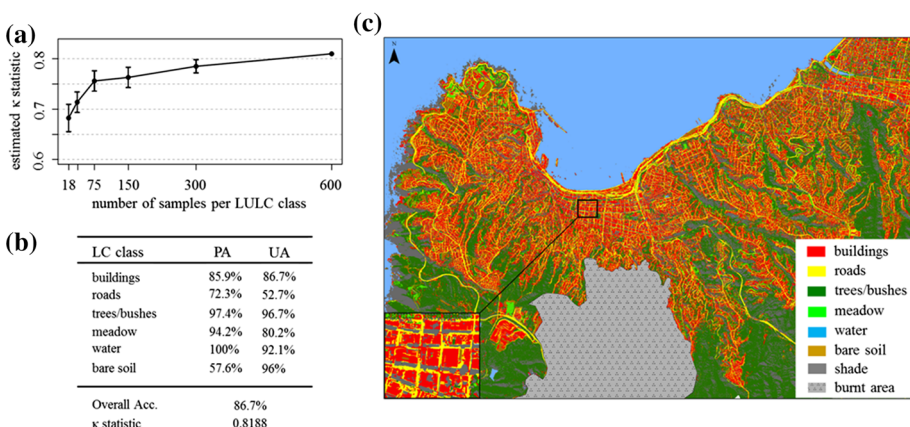


Fig. 9 Results from LULC information extraction workflow; **a** estimated κ statistic of different model runs (reported as mean and standard deviation based on 10 independent runs) with varying number of labeled training segments per class included; **b** accuracy measures for final LULC classification after postclassification processing (PA Producer's accuracy, UA user's accuracy); **c** final LULC classification map

respectively. In particular, the mutual confusion of the spectrally overlapping classes “buildings” and “roads” could be decreased. From the accuracies of individual classes, it can be noted that the vegetation-related classes and “water” feature highest accuracies. However, also the class “buildings” features very high values, which could be improved notably by the postclassification processing procedure: The final classification features an enhanced producer’s accuracy of 85.9% (+1.2%) and a user’s accuracy of 86.7% (+2.8%) for this class, which underlines the viability of the proposed information extraction workflow in this challenging empirical setting.

4.2 Exposure estimation

4.2.1 Number of buildings

For validation purposes, 25 grid cells, which do not belong to the training set, are selected randomly, and the actual number of buildings is determined by manual image interpretation. Performance of models is assessed with a set of measures, which comprises Pearson product-moment correlation coefficient (R), mean absolute error (MAE), RMSE, relative absolute error (RAE), root relative squared error (RRSE), and mean absolute percentage error (MAPE) (Fig. 10a). It can be noted that negative or super-positive prediction values were pruned from the models’ output to ensure physically meaningful values for building number estimation. Pruned values are related to non-complete LULC information for individual grid cells at boarder regions of the settlement area, which were in addition subject to LULC misclassifications. Hence, numerical values of metrics characterizing the individual grid cells are beyond the known training space, which leads to improper extrapolation (Okujeni et al. 2013).

It can be seen from Fig. 10a that both models feature a very high additive relationship between predictions and reference ($R > 0.8$), especially given the limited amount of labeled grid cells for establishing the models. MAE of the number of estimated buildings from the reference data set is 26 buildings for the OLS model and less than 22 buildings for the SVR model, which corresponds in relative terms (MAPE) to a deviation of 35.7% (OLS) and 26.2% (SVR). In accordance with the values of aforementioned measures, also

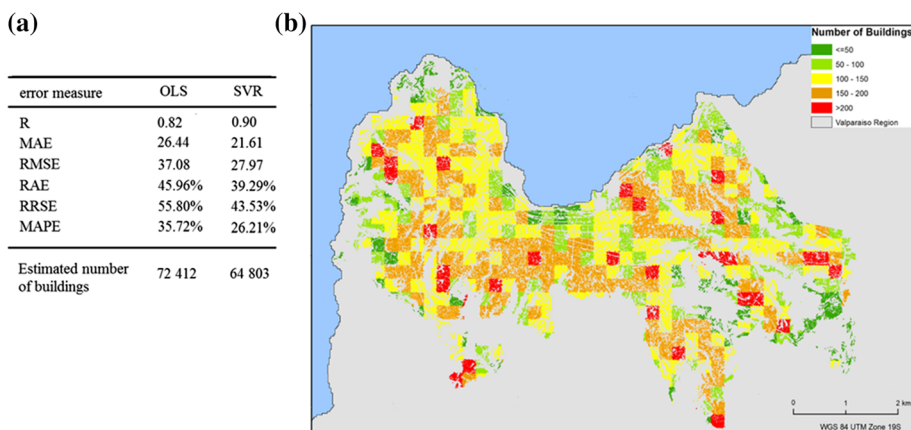


Fig. 10 Results of estimations of number of buildings; **a** different error measures for both OLS and SVR model; **b** applied SVR model for Valparaíso

RMSE, which represents an important criterion to assess the quality of fit of a prediction model, underlines that the SVR model performs better. It can also be noted that a rather small difference between MAE and RMSE corresponds to an insignificant influence (i.e., nonexistence) of outliers (i.e., large deviations). This underlines again the superiority of the SVR model in conjunction with the residual relative error measures.

Figure 10b illustrates the results from the applied SVR model for the city of Valparaíso. Overall, 64,803 buildings are predicted by the SVR model for the pictured area (approximately 7600 less than the OLS model). In accordance with the error measures, also the application of the model features a reasonable output. For instance, the harbor area and city center are characterized by a low number of buildings, since there dominantly very large buildings with industrial or commercial use exist. Instead, the hill quarters feature many small buildings with residential use and are thus characterized by a high number of buildings (see also Fig. 1c). In this sense, both examples are directly reflected by the model outputs. Thus, we conclude that the number of buildings as crucial information on exposure is derived in its correct dimension and that the approach can be evaluated as feasible in this setting.

4.2.2 Population disaggregation

Validation of the population disaggregation is based on the finest level of available census data (i.e., “manzanas”/building blocks). Therefore, the results of the target zone on pixel level are aggregated to the corresponding building block geometries for comparison. With respect to the MAE, we observe an increase in accuracy given our baseline method (MAE of SAW: 46.14) when incorporating estimated number of buildings (MAE of SAW-NB: 42.69). Notably, the accuracy levels of both approaches increase, when information from OSM is included (i.e., MAE of SAW OSM: 43.37, MAE of SAW-NB OSM: 41.77). To get more differentiated insights, we plotted MAEs of different methods according to the population size of the respective reference building block (Fig. 11a). It can be seen that

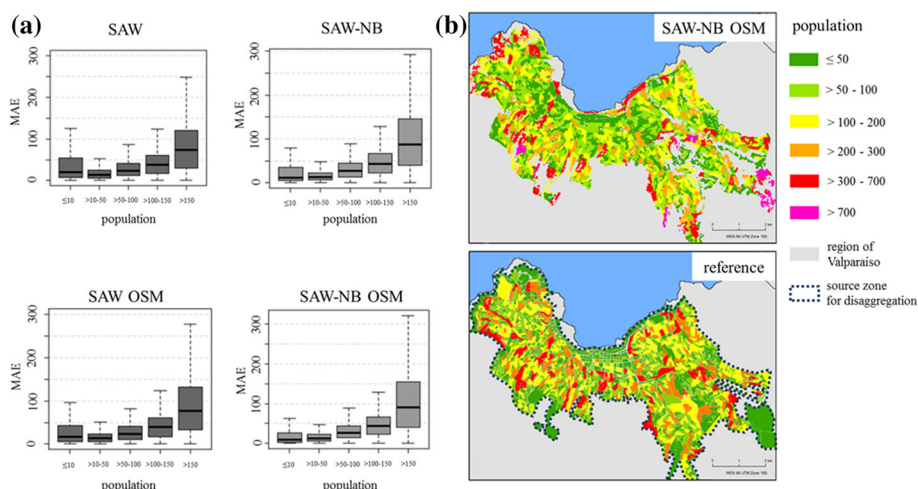


Fig. 11 Results of population estimation; **a** box plots of mean absolute errors according to population size of reference building block with respect to different methods; **b** population disaggregation based on simple areal weighting under consideration of estimated number of buildings and land-use information from OSM (SAW-NB OSM); reference on building block level

low populated and, more significantly, high populated areas appear to be prone to erroneous estimations. The interquartile range of highly populated areas is distinctively large, which indicates that errors can be both quite low and extremely high. When manually inspecting the results, it becomes apparent that large deviations can be primarily attributed to the number of (large) multi-story buildings within a building block (i.e., building blocks feature a high number of people in the reference but not a correspondingly high number in the estimation result). Such relations can hardly be reflected given the deployed two-dimensional remote sensing data. However, the incorporation of height information from, for example, a normalized digital surface model could be employed to substantially increase the level of accuracy (Aubrecht et al. 2009). Nevertheless, beside those outliers, MAEs of the estimates reflect overall a fair correspondence with respect to the reference.

The corresponding population map of the best performing method (i.e., SAW-NB OSM) is depicted in Fig. 11b along with the population numbers of the reference blocks. Most noticeable areas of overestimation are located at large sports and health areas in the Northwest, and at the airfield in the Southeast of the city, which can be primarily attributed to misclassifications. Nevertheless, the overall allocation of population reflects the spatial distribution of the reference, especially given the circumstance that the number of population was disaggregated from the coarsest level of census data available (i.e., a single number was available for the source zone which comprises the whole city of Valparaíso). In this regard, it can be noted that especially large shares of the population of the tsunami-prone harbor region can be reflected properly. Thereby, helpful information could be encoded from the OSM data in terms of “land-use objects” and POIs for this area (Fig. 8) to improve the mapping results. This underlines again the usefulness of incorporation of OSM information.

4.2.3 Application for tsunami scenario

To demonstrate the relevance of the presented approaches in the context of natural hazard risk, we compute the today’s number of affected buildings and people for a historically grounded tsunami scenario. In particular, we consider the destructive tsunami event from 1730. The tsunami was triggered by an earthquake with an approximate magnitude M_w of 9.0 (Cisternas et al. 2012) and inundated the lower coastal parts of the settlement area of Valparaíso. The inundation area from Fig. 12 was obtained with a numeric modeling approach under consideration of topographic, bathymetric, and seismic data (SHOA 2012, 2015). The modeling results can be partly verified by taking into consideration marks at historical places (i.e., iglesia de la Matriz, and iglesia de la Merced), which represent documented borders of the inundation and confirm the viability of the inundation model. The severity of the inundation becomes in particular obvious when compared with the inundation line of the 1906 tsunami. According to the number of buildings (Fig. 10) and people (Fig. 11) estimated previously, a similar event would affect nowadays approximately 2900 buildings and 9300 people (according to their place of residence, i.e., during a nighttime event).

5 Conclusions and future perspectives

In this paper, we presented a novel workflow for the estimation of important exposure characteristics by joint exploitation of VHR remote sensing data and VGI. Thereby, OSM data were deployed in three different key applications: LULC classification, estimation of

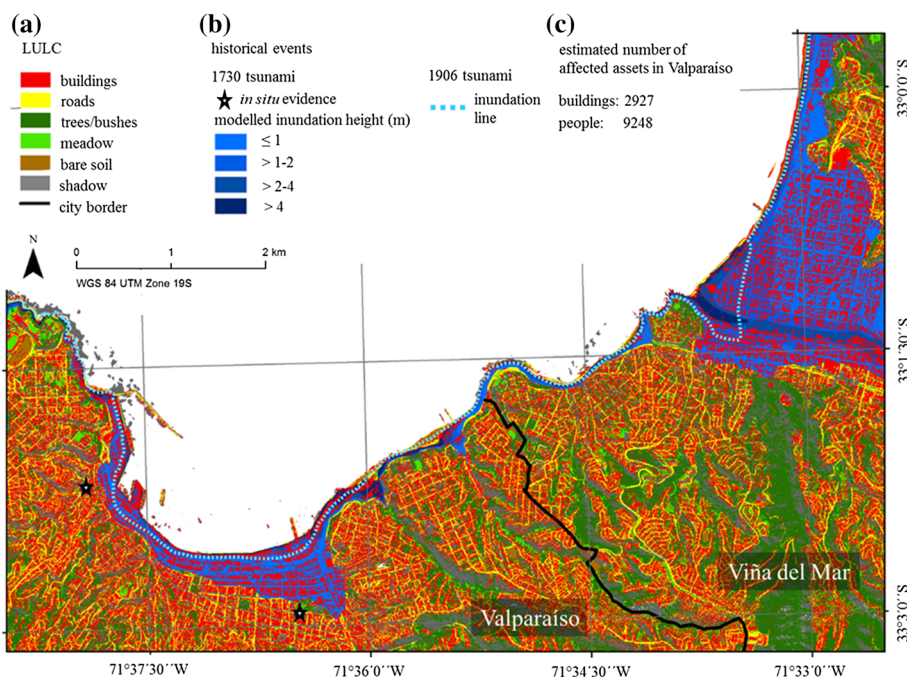


Fig. 12 Tsunami scenario for Valparaíso and Viña del Mar; **a** LULC classes and city borders; **b** characteristics of historical tsunami events; **c** estimated number of affected assets for the city of Valparaíso

number of buildings, and estimation of exposed population. To this purpose, labeled training samples were generated from the OSM data for supervised LULC classification in conjunction with remote sensing imagery. Thereby, a spatially constrained selection of most viable samples was carried out under consideration of OSM data-related quality measures. LULC classification results obtained with a rotation forest model featured excellent κ statistics above 0.8. Analogously, viable estimation of number of buildings could be achieved by establishing an empirical relation between the number of building geometries from the OSM data and affiliated LULC information. Finally, OSM data proved also useful for the enhancement of accuracy of population disaggregation approaches. In summary, this study underlines the potential of incorporating VGI in remote sensing applications for information extraction procedures and exposure estimation, which can be in particular useful in data-scarce regions of the world. Thereby, improved results can be expected when anticipating a likely increase in availability and quality of VGI data in the future.

In this manner, future work is suggested to address the development of advanced approaches to assess the quality and credibility of VGI data. This would be an important step toward fully automated processing systems. In addition, other sources containing georeferenced information such as Twitter, Flickr or Wikimapia can be explored for extended analysis (Blaschke et al. 2011). Recent conceptual works explicitly acknowledge temporal aspects (Volunteered Geo-Dynamic Information) and describe the potential impact on the field of dynamic population distribution modeling to overcome limits of residency-based census data (Aubrecht et al. 2016). As just one example, Aubrecht et al. (2011) deploy VGI from a location sharing service to characterize the dynamics of

population patterns. Moreover, it would be interesting to examine to what extent VGI can contribute to the assessment of other components of natural hazard risks, such as seismic vulnerability of built environments with respect to earthquakes, in conjunction with the application of remote sensing (Geiß et al. 2014, 2015, 2016a). This could serve as important information for comprehensive risk and damage assessments in the context of, for example, earthquakes (Picozzi et al. 2013) or tsunamis (Strunz et al. 2011; Wegscheider et al. 2011; Gokon et al. 2015) for prospective multi-hazard early warning and response systems.

Generally, we believe that a combined use of remote sensing, as a powerful earth monitoring tool, and VGI, as an exhaustive information source, has the potential to contribute substantially to the generation and updating of global risk models—for enhanced disaster mitigation and response.

Acknowledgements The authors would like to acknowledge the support by the German Federal Ministry for Education and Research (BMBF), under Grant Agreement No. 01DN12089. This work was also supported by the Helmholtz Association under the framework of the Postdoc project “pre_DICT” (PD-305). The authors would like to thank European Space Imaging (EUSI) for providing WorldView-2 imagery and the anonymous reviewers for the helpful comments.

References

- Adeline KRM, Chen M, Briottet X, Pang SK, Paparoditis N (2013) Shadow detection in very high spatial resolution aerial images: a comparative study. *ISPRS J Photogramm Remote Sens* 80:21–38
- Ali M, Clausi D (2001) Using the Canny edge detector for feature extraction and enhancement of remote sensing images, IGARSS 2001. Scanning the present and resolving the future. In: Proceedings of IEEE 2001 international geoscience and remote sensing symposium, vol 5(C), pp 2298–2300
- Aubrecht C, Steinnocher K, Hollaus M, Wagner W (2009) Integrating earth observation and GIScience for high resolution spatial and functional modeling of urban land use. *Comput Environ Urban Syst* 33(1):15–25
- Aubrecht C, Ungar J, Freire S (2011) Exploring the potential of volunteered geographic information for modeling spatio-temporal characteristics of urban population A case study for Lisbon Metro using foursquare check-in data. International conference virtual city and territory 2011, Lisboa, pp 11–13
- Aubrecht C, Özceylan D, Steinnocher K, Freire S (2013) Multi-level geospatial modeling of human exposure patterns and vulnerability indicators. *Nat Hazards* 68:147–163
- Aubrecht C, Özceylan D, Ungar J, Freire S, Steinnocher K (2016) VGDI—advancing the concept: volunteered geo-dynamic information and its benefits for population dynamics modeling. *Trans GIS*. doi:[10.1111/tgis.12203](https://doi.org/10.1111/tgis.12203)
- Baatz M, Schäpe A (2000) Multiresolution segmentation—an optimization approach for high quality multi-scale image segmentation. In: Strobl J, Blaschke T, Griesebner G (eds) *Angewandte Geographische Informations-Verarbeitung XII*. Wichmann Verlag, Karlsruhe, pp 12–23
- Belgiu M, Dragut L (2014) Comparing supervised and unsupervised multiresolution segmentation approaches for extracting buildings from very high resolution imagery. *ISPRS J Photogramm Remote Sens* 96:67–75
- Berry JK (2007) Map analysis: understanding the spatial patterns and relationships. GeoTec Media, San Francisco
- Bianchini R, Feeney G, Rajendra S (2013) Report of the International Commission on the 2012 Population and Housing Census of Chile. Technical Report November, International Commission, Santiago de Chile
- Blaschke T (2010) Object based image analysis for remote sensing. *ISPRS J Photogramm Remote Sens* 65:2–16
- Blaschke T, Hay G, Weng Q, Resch B (2011) Collective sensing: integrating geospatial technologies to understand urban systems—an overview. *Remote Sens* 3(8):1743–1776
- Bruzzone L, Carlin L (2006) A multilevel context-based system for classification of very high spatial resolution images. *IEEE Trans Geosci Remote Sens* 44(9):2587–2600

- Bruzzone L, Chi M, Marconcini M (2006) A Novel transductive SVM for semisupervised classification of remote-sensing images. *IEEE Trans Geosci Remote Sens* 44(11):3363–3373
- Burges CJC (1998) A tutorial on support vector machines for pattern recognition. *Data Min Knowl Disc* 2:1–47
- Camps-Valls G, Tuia D, Bruzzone L, Benediktsson JA (2014) Advances in hyperspectral image classification: earth monitoring with statistical learning methods. *IEEE Signal Process Mag* 31(10):45–54
- Canny J (1986) A computational approach to edge detection. *IEEE Trans Pattern Anal Mach Intell* 8(6):679–698
- Chen CH, Ho PGP (2008) Statistical pattern recognition in remote sensing. *Pattern Recogn* 41(9):2731–2741
- Cisternas M, Torrejón F, Gorigoitia N (2012) Amending and complicating Chile's seismic catalog with the Santiago earthquake of 7 August 1580. *J S Am Earth Sci* 33:102–109
- Cortes C, Vapnik V (1995) Support vector networks. *Mach Learn* 20:1–25
- Cutter S (2003) Social Vulnerability to environmental hazards. *Soc Sci Q* 84(2):242–261
- Demir B, Minello L, Bruzzone L (2014) Definition of effective training sets for supervised classification of remote sensing images by a novel cost-sensitive active learning method. *IEEE Trans Geosci Remote Sens* 52(2):1272–1284
- DigitalGlobe (2010) The benefits of the eight spectral bands of WorldView-2. Whitepaper. https://www.digitalglobe.com/sites/default/files/DG-8SPECTRAL-WP_0.pdf. Accessed 6 July 2015
- Dragut L, Tiede D, Levick SR (2010) ESP: a tool to estimate scale parameter for multiresolution image segmentation of remotely sensed data. *Int J Geogr Inf Sci* 24(6):859–871
- Ehrlich D, Tenerelli P (2013) Optical satellite imagery for quantifying spatio-temporal dimension of physical exposure in disaster risk assessments. *Nat Hazards* 68:1271–1289
- Ehrlich D, Zeug G, Gallego J, Gerhardinger A, Caravaggi I, Pesaresi M (2010) Quantifying the building stock from optical high-resolution satellite imagery for assessing disaster risk. *Geocarto Int* 25(4):281–293
- Ehrlich D, Kemper T, Blaes X, Soille P (2013) Extracting building stock information from optical satellite imagery for mapping earthquake exposure and its vulnerability. *Nat Hazards* 68:79–95
- Epifanio I, Soille P (2007) Morphological texture features for unsupervised and supervised segmentations of natural landscapes. *IEEE Trans Geosci Remote Sens* 45(4):1074–1083
- Esch T, Thiel M, Bock M, Roth A, Dech S (2008) Improvement of image segmentation accuracy based on multiscale optimization procedure. *IEEE Geosci Remote Sens Lett* 5(3):463–467
- Espindola GM, Camara G, Reis IA, Bins LS, Monteiro AM (2006) Parameter selection for region-growing image segmentation algorithms using spatial autocorrelation. *Int J Remote Sens* 27(14):3035–3040
- Fan H, Zipf A, Fu Q, Neis P (2014) Quality assessment for building footprints data on OpenStreetMap. *Int J Geogr Inf Sci* 28(4):700–719
- Flanagan AJ, Metzger MJ (2008) The credibility of volunteered geographic information. *GeoJournal* 72(3–4):137–148
- Foody GM (2002) Status of land cover classification accuracy assessment. *Remote Sens Environ* 80:185–201
- Foody GM, Boyd DS (2013) Using volunteered data in land cover map validation: mapping west African forests. *IEEE J Sel Top Appl Earth Obs Remote Sens* 6(3):1305–1312
- Geiß C, Taubenböck H (2013) Remote sensing contributing to assess earthquake risk: from a literature review towards a roadmap. *Nat Hazards* 68:7–48
- Geiß C, Taubenböck H (2015) Object-based Postclassification Relearning. *IEEE Geosci Remote Sens Lett* 12(11):2336–2340
- Geiß C, Taubenböck H, Tyagunov S, Tisch A, Post J, Lakes T (2014) Assessment of seismic building vulnerability from space. *Earthq Spectra* 30(4):1553–1583
- Geiß C, Pelizari PA, Marconcini M, Sengara W, Edwards M, Lakes T, Taubenböck H (2015) Estimation of seismic building structural types using multi-sensor remote sensing and machine learning techniques. *ISPRS J Photogramm Remote Sens* 104:175–188
- Geiß C, Jilge M, Lakes T, Taubenböck H (2016a) Estimation of seismic vulnerability levels of urban structures with multisensor remote sensing. *IEEE J Sel Top Appl Earth Obs Remote Sens* 9(5):1913–1936
- Geiß C, Klotz M, Schmitt A, Taubenböck H (2016b) Object-based morphological profiles for classification of remote sensing imagery. *IEEE Trans Geosci Remote Sens* 54(10):5952–5963
- Geofabrik (2014) OpenStreetMap Data Extracts. <http://download.geofabrik.de/>. Accessed 5 Nov 2014
- Gokon H, Post J, Stein E, Martinis S, Twele A, Mück M, Geiß C, Koshimura S, Matsuoka M (2015) A method for detecting buildings destroyed by the 2011 Tohoku earthquake and tsunami using multi-temporal TerraSAR-X data. *IEEE Geosci Remote Sens Lett* 12(6):1277–1281
- Goodchild MF (2007) Citizens as sensors: the world of volunteered geography. *GeoJournal* 69(4):211–221

- Haklay M (2010) How good is volunteered geographical information? A comparative study of OpenStreetMap and ordnance survey datasets. *Environ Plan* 37(4):682–703
- Hall M, Frank E, Holmes G, Pfahringer B, Reutemann P, Witten IH (2009) The WEKA data mining software: an update. *SIGKDD Explor* 11(1):10–18
- Hecht R, Kunze C, Hahmann S (2013) Measuring completeness of building footprints in OpenStreetMap over space and time. *ISPRS Int J Geo Inf* 2(4):1066–1091
- Indirli M, Valpreda E, Panza G, Romanelli F, Lanzoni L, Teston S, Berti M, Bennardo SD, Rossi G (2010) Natural multi-hazard and building vulnerability assessment in the historical centers: the examples of San Giuliano di Puglia (Italy) and Valparaíso (Chile). In: Proceedings of the European commission conference “SAUVEUR”, safeguarded cultural heritage, May 31–June 3, Praha
- INE (2015) Instituto Nacional de Estadísticas Chile: Estadísticas Chile. http://www.ine.cl/canales/chile_estadistico/familias/censos.php. Accessed 22 Jan 2015
- Jokar Arsanjani J, Helbich M, Bakillah M, Loos L (2015a) The emergence and evolution of OpenStreetMap: a cellular automata approach. *Int J Digit Earth* 8(1):74–88
- Jokar Arsanjani J, Zipf A, Mooney P, Helbich M (eds) (2015b) An introduction to OpenStreetMap in GIScience: experiences, research, applications. In: *OpenStreetMap in GIScience: experiences, research, applications*. Springer, Switzerland
- Jokar Arsanjani J, Mooney P, Helbich M, Zipf A (2015c) An exploration of future patterns of the contributions to OpenStreetMap and development of a contribution index. *Trans GIS*. doi:[10.1111/tgis.1213](https://doi.org/10.1111/tgis.1213)
- Kavzoglu T, Colkesen I (2013) An assessment of the effectiveness of a rotation forest ensemble for land-use and land-cover mapping. *Int J Remote Sens* 34(12):4224–4241
- Klonner C, Barron C, Neis P, Höfle B (2014) Updating digital elevation models via change detection and fusion of human and remote sensor data in urban environments. *Int J Digit Earth* 8(2):151–169
- Kunze C, Hecht R (2015) Semantic enrichment of building data with volunteered geographic information to improve mappings of dwelling units and population. *Comput Environ Urban Syst*. doi:[10.1016/j.compenvurbsys.2015.04.002](https://doi.org/10.1016/j.compenvurbsys.2015.04.002)
- Lee JS (1983) Digital image smoothing and the sigma filter. *Comput Vis Graph* 24(2):255–269
- Leichtle T, Geiß C, Wurm M, Lakes T, Taubenböck H (2017) Unsupervised change detection in VHR remote sensing imagery—an object-based clustering approach in a dynamic urban environment. *Int J Appl Earth Obs Geoinf* 54:15–27
- Mack B, Roscher R, Waske B (2014) Can i trust my one-class classification? *Remote Sens* 6(9):8779–8802
- Marconcini M, Fernandez-Prieto D, Buchholz T (2014) Targeted land-cover classification. *IEEE Trans Geosci Remote Sens* 52(7):4173–4193
- Martha TR, Kerle N, van Westen CJ, Jetten V, Kumar KV (2011) Segment optimization and data-driven thresholding for knowledge-based landslide detection by object-based image analysis. *IEEE Trans Geosci Remote Sens* 49(12):4928–4943
- Mennis J, Hultgren T (2006) Intelligent dasymetric mapping and its application to areal interpolation. *Cartogr Geogr Inf Sci* 33(3):179–194
- Montgomery DC, Peck EA, Vining GG (2001) Introduction to linear regression analysis, 3rd edn. Wiley, New York, p 672
- Neis P, Zipf A (2012) Analyzing the contributor activity of a volunteered geographic information project—the case of OpenStreetMap. *ISPRS Int J Geo Inf* 1(3):146–165
- Okujeni A, van der Linden S, Tits L, Somers B, Hostert P (2013) Support vector regression and synthetically mixed training data for quantifying urban land cover. *Remote Sens Environ* 137:184–197
- ONEMI (2014) Ministerio de Interior y Seguridad Pública: Incendio en Valparaíso. <http://www.onemi.cl/incendio-en-valparaiso>. Accessed 22 Jan 2015
- OSM Task Manager (2014a) #502—Valparaíso, Chile Fires/Fuegos en Valparaíso, Chile. <http://tasks.hotosm.org/project/502>. Accessed 22 Jan 2015
- OSM Task Manager (2014b) #508—Valparaíso, Chile Fires 2/Valparaíso, Chile Incendios. <http://tasks.hotosm.org/project/508>. Accessed 22 Jan 2015
- OSM (2015a) OpenStreetMap copyright. <http://www.openstreetmap.org/copyright/en>. Accessed 26 June 2015
- OSM (2015b) OpenStreetMap Map Features. http://wiki.openstreetmap.org/wiki/Map_Features. Accessed 13 Jan 2015
- OSM (2015c) Planet.osm. <http://wiki.openstreetmap.org/wiki/Planet.osm>. Accessed 22 Jan 2015
- Pasolli E, Melgani F, Tuia D, Pacifici F, Emery WJ (2014) SVM active learning approach for image classification using spatial information. *IEEE Trans Geosci Remote Sens* 52(4):2217–2233
- Pesaresi M, Benediktsson J (2001) A new approach for the morphological segmentation of high-resolution satellite imagery. *IEEE Trans Geosci Remote Sens* 39(2):309–320

- Pesaresi M, Huadong G, Blaes X, Ehrlich D, Ferri S, Gueguen L, Halkia M, Kauffmann M, Kemper T, Lu L, Marin-Herrera MA, Ouzounis GK, Scavazzon M, Soille P, Syrris V, Zanchetta L (2013) A global human settlement layer from optical HR/VHR RS data: concept and first results. *IEEE J Sel Top Appl Earth Obs Remote Sens* 6(5):2102–2131
- Picoczi M, Bindi D, Pittore M, Kieling K, Parolai S (2013) Real-time risk assessment in seismic early warning and rapid response: a feasibility study in Bishkek (Kyrgyzstan). *J Seismol* 17:485–505
- Poser K, Dransch D (2010) Volunteered geographic information for disaster management with application to rapid flood damage estimation. *Geomatica* 64(1):89–98
- Puissant A, Rougier S, Stumpf A (2014) Object-oriented mapping of urban trees using Random Forest classifiers. *Int J Appl Earth Obs Geoinf* 26:235–245
- Richter R (1996) A spatially adaptive fast atmospheric correction algorithm. *Int J Remote Sens* 17(6):1201–1214
- Richter R, Schläpfer D (2014) Atmospheric/topographic correction for satellite imagery, Technical report Rodriguez JJ, Kuncheva LI, Alonso CJ (2006) Rotation forest: a new classifier ensemble method. *IEEE Trans Pattern Anal Mach Intell* 28(10):1619–1630
- Sánchez MA, Bosque MJ, Jiménez VC (2009) Valparaíso: su geografía, su historia y su identidad como Patrimonio de la Humanidad. *Estudios Geográficos* 70(266):269–293
- Schnenebele E, Cervone G (2013) Improving remote sensing flood assessment using volunteered geographical data. *Nat Hazard Earth Syst Sci* 13(3):669–677
- Schneiderbauer S, Ehrlich D (2004) Risk, hazard and people's vulnerability to natural hazards. A review of definitions, concepts and data. Joint Research Centre, European Commission, EUR 21410
- Sester M, Arsanjani JJ, Klammer R, Burghardt D, Haunert JH (2014) Integrating and generalizing volunteered geographic information. In: Duchene B, Mackaness C, Burghardt W (eds) *Abstracting geographic information in a data rich world*. Springer Press, Cham
- Sheng LSL, Xiaoyu WXW, Xinfa QXQ, Yongjian HYH (2009) Mathematical morphology edge detection algorithm of remote sensing image with high resolution. 2009 1st International conference on information science and engineering (ICISE), pp 1323–1326
- SHOA (2012) Carta de Inundación por Tsunami para Valparaíso—Viña del Mar: referida al evento de 1730. http://www.shoa.cl/servicios/citsu/pdf/citsu_valparaiso_vinna.pdf. Accessed 20 Oct 2015
- SHOA (2015) Instrucciones Oceanográficas No 4 “Especificaciones Técnicas para la Elaboración de Cartas de Inundación por Tsunami (CITSU)”. Pub. SHOA 3204
- Smola AJ, Schölkopf B (2004) A tutorial on support vector regression. *Stat Comput* 14:199–222
- Soille P (2004) Morphological image analysis, 2nd edn. Springer-Verlag, Berlin
- Soille P, Pesaresi M (2002) Advances in mathematical morphology applied to geoscience and remote sensing. *IEEE Trans Geosci Remote Sens* 40(9):2042–2055
- Stiglic G, Rodriguez JJ, Kokol P (2011) Rotation of Random Forests for genomic and proteomic classification problems. *Adv Exp Med Biol* 696:211–221
- Strunz G, Post J, Zosseder K, Wegscheider S, Mück M, Riedlinger T, Mehl H, Dech S, Birkmann J, Gebert N, Harjono H, Anwar HZ, Sumaryono Khomarudin RM, Muhari A (2011) Tsunami risk assessment in Indonesia. *Nat Hazards Earth Syst Sci* 11:67–82
- Stumpf A, Kerle N (2011) Object-oriented mapping of landslides using Random Forests. *Remote Sens Environ* 115(10):2564–2577
- Stumpf A, Lachiche N, Malet JP, Kerle N, Puissant A (2014) Active learning in the spatial domain for remote sensing image classification. *IEEE Trans Geosci Remote Sens* 52(5):2492–2507
- Sun Z, Fang H, Deng M, Chen A, Yue P, Di L (2015) Regular shape similarity index: a novel index for accurate extraction of regular objects from remote sensing images. *IEEE Trans Geosci Remote Sens* 53(7):3737–3748
- Taubenböck H, Post J, Roth A, Zosseder K, Strunz G, Dech S (2008) A conceptual vulnerability and risk framework as outline to identify capabilities of remote sensing. *Nat Hazards Earth Syst Sci* 8(3):409–420
- Taubenböck H, Esch T, Wurm M, Roth A, Dech S (2010) Object-based feature extraction using high spatial resolution satellite data of urban areas. *J Spatial Sci* 55(1):117–133
- Taubenböck H, Esch T, Felbier A, Wiesner M, Roth A, Dech S (2012) Monitoring urbanization in mega cities from space. *Remote Sens Environ* 117:162–176
- Taubenböck H, Klotz M, Wurm M, Schmieder J, Wagner B, Wooster M, Esch T, Dech S (2013) Delineation of Central Business Districts in mega city regions using remotely sensed data. *Remote Sens Environ* 136:386–401
- Thywissen K (2006) Core terminology of disaster reduction: a comparative glossary. In: Birkmann J (ed) *Measuring vulnerability to natural hazards*. United Nations University Press, New York, pp 448–496

- Timmermann P (1981) Vulnerability, resilience and the collapse of society. No. 1 in environmental monograph. Institute for Environmental Studies, University of Toronto
- Trimble (2014) eCognition developer 9.0 reference book. Germany Trimble Documentation, München
- Tuia D, Pacifici F, Kanevski M, Emery WJ (2009a) Classification of very high spatial resolution imagery using mathematical morphology and support vector machines. *IEEE Trans Geosci Remote Sens* 47(11):3866–3879
- Tuia D, Ratle F, Pacifici F, Kanevski MF, Emery WJ (2009b) Active learning methods for remote sensing image classification. *IEEE Trans Geosci Remote Sens* 47(7):2218–2232
- Tuia D, Copo L, Kanevski M, Munoz-Mari J (2011a) A survey of active learning algorithms for supervised remote sensing image classification. *IEEE J Sel Top Signal Process* 5(3):606–617
- Tuia D, Pasolli E, Emery WJ (2011b) Using active learning to adapt remote sensing image classifiers. *Remote Sens Environ* 115(9):2232–2242
- UNDRO (1979) Natural disasters and vulnerability analysis. Report of Expert Group Meeting, Geneva, 9–12 July 1979
- Vapnik VN (1995) The nature of statistical learning theory. Springer, New York, p 187
- Wegscheider S, Post J, Zosseder K, Mück M, Strunz G, Riedlinger T, Muhari A, Anwar HZ (2011) Generating tsunami risk knowledge at community level as a base for planning and implementation of risk reduction strategies. *Nat Hazards Earth Syst Sci* 11:249–258
- Wieland M, Pittore M, Parolai S, Zschau J (2012a) Exposure estimation from multi-resolution optical satellite imagery for seismic risk assessment. *ISPRS Int J GeoInf* 1:69–88
- Wieland M, Pittore M, Parolai S, Zschau J, Moldobekov B, Begaliev U (2012b) Estimating building inventory for rapid seismic vulnerability assessment: towards an integrated approach based on multi-source imaging. *Soil Dyn Earthq Eng* 36:70–83
- Wu S-S, Qiu X, Wang L (2005) Population estimation methods in GIS and remote sensing: a review. *GISci Remote Sens* 42(1):58–74
- Xia J, Du P, He X, Chanussot J (2014) Hyperspectral remote sensing image classification based on rotation forest. *IEEE Geosci Remote Sens Lett* 11(1):239–243
- Xia J, Chanussot J, Du P, He X (2015) Spectral-spatial classification for hyperspectral data using rotation forests with local feature extraction and markov random fields. *IEEE Trans Geosci Remote Sens* 53(5):2532–2546
- Zheng L, Wan L, Huo H, Fang T (2014) A noise removal approach for object-based classification of VHR imagery via post-classification. 2014 International conference on audio, language and image processing, pp 915–920
- Zielstra D, Zipf A (2010) A comparative study of proprietary geodata and volunteered geographic information for Germany. In: Proceedings of 13th AGILE international conference on geographic information science, vol 1, 10–14 May, Guimarães